Decay rates of almost strong modes in Floquet spin chains beyond Fermi's Golden Rule

Hsiu-Chung Yeh,[1] Achim Rosch,[2] and Aditi Mitra[1]
[1]*Center for Quantum Phenomena, Department of Physics, New York University, 726 Broadway, New York, New York 10003, USA*
[2]*Institute for Theoretical Physics, University of Cologne, 50937 Cologne, Germany*

(Received 8 May 2023; revised 12 July 2023; accepted 25 July 2023; published 4 August 2023)

The stability and dynamics of almost strong zero and π modes in weakly nonintegrable Floquet spin chains are investigated. Such modes can also be viewed as localized Majorana modes at the edge of a topological superconductor. Perturbation theory in the strength of integrability breaking interaction J_z is employed to estimate the decay rates of these modes, and compared to decay rates obtained from exact diagonalization. The structure of the perturbation theory and thus the lifetime of the modes is governed by the conservation of quasienergy modulo $2\pi/T$, where T is the period of the Floquet system. If there are $4n-1$ bulk excitations whose quasienergies add up to zero (or π/T for a π mode), one obtains a decay channel of the Majorana mode with a decay rate proportional to J_z^{2n}. Thus the lifetime is sensitively controlled by the width of the single-particle Floquet bands. For regimes where the decay rates are quadratic in J_z, an analytic expression for the decay rate in terms of an infinite temperature autocorrelation function of the integrable model is derived, and shown to agree well with exact diagonalization.

DOI: 10.1103/PhysRevB.108.075112

I. INTRODUCTION

The study of topological phenomena is a frontier topic in condensed matter physics, with the classification of topological phases showing further enrichment under periodic or Floquet driving [1,2]. At the single-particle level, topological phenomena are well understood, with the defining characteristics being a bulk boundary correspondence, where a nonzero bulk topological invariant predicts the number of edge modes. However, the effect of weak interactions on the stability of edge modes in topological systems in general, and Floquet topological systems in particular, is not fully understood. With Floquet driving and interactions, the system is susceptible to heating, and one might naively expect all edge physics to quickly melt away on the same time scales as typical bulk observables heat. Nevertheless, if the system hosts strong modes [3–18], typically encountered at the edge of certain one-dimensional systems, the edge modes can be stable over time scales much longer than bulk heating times [7,8,11–16].

For Floquet systems with Z_2 symmetry, strong modes are of two kinds, zero modes that are local Majorana operators that commute with a Floquet unitary, and π modes that are local Majorana operators that anticommute with the Floquet unitary [11,19–24]. Since this property is not tied to any eigenstate of the system, any Floquet eigenstate with open boundary conditions can show signatures of these edge modes. These strong modes also anticommute with the Z_2 symmetry leading to eigenspectrum phases. In particular, the zero mode implies each eigenstate is at least doubly degenerate with the degenerate pairs being even and odd under parity (Z_2 symmetry), while the π mode implies every even parity eigenstate has an odd parity partner whose quasienergy is larger than the former by π/T (modulo $2\pi/T$), where T is the Floquet period.

So far, all Floquet spin chains for which strong modes have been derived can be represented as unitaries of fermion bilinears [11,20]. Besides an exact construction of the operators, strong modes can also be detected by studying the infinite temperature autocorrelation function of an operator on the edge [7,11–14]. If a strong mode exists, and the operator has an overlap with it, then the infinite temperature autocorrelation function is long lived, with a lifetime that grows exponentially with system size [4,5]. This approach can easily be extended to nonintegrable Floquet spin chains [15,16], where the nonintegrability is via the application of unitaries of four-fermion interactions. In this case, one expects that the correlation function does ultimately decay but possibly after a very long time.

Employing the diagnostic of the autocorrelation function, obtaining the interaction dependent lifetime can be notoriously difficult, especially when the integrability breaking is very weak [25]. This is because, for weak integrability breaking, the decay is primarily due to finite-size effects, with the system sizes needed to be in a regime where the decay is controlled purely by the integrablity breaking terms, being much too large. For this reason, for weakly nonintegrable systems, these edge modes are referred to as almost strong modes (ASM) [7,8,11–14]. In this paper we explore to what extent perturbation theory can help estimate the decay times of almost strong modes of weakly nonintegrable Floquet spin chains. We identity regimes where Fermi's golden rule (FGR) is valid, and also regimes where FGR breaks down and higher powers of the integrability breaking term are needed to capture the decay.

The paper is organized as follows. We introduce the model in Sec. II, summarizing the essential properties in the integrable limit, and introducing the infinite temperature autocorrelation function. In Sec. III we derive the FGR decay rates in terms of an appropriate infinite temperature autocorrelation function of the integrable model. We also highlight regimes where FGR breaks down and we present a simple argument

to determine what powers of the integrability breaking term control the decay. In Sec. IV we present the numerical results and compare them to theoretical predictions. We present our conclusions in Sec. V, while intermediate steps in the derivations are relegated to the Appendixes.

II. MODEL

We study stroboscopic time evolution of an open chain of length L according to the Floquet unitary

$$U = e^{-i\frac{T}{2}J_z H_{zz}} e^{-i\frac{T}{2}gH_z} e^{-i\frac{T}{2}J_x H_{xx}}, \tag{1}$$

where

$$H_{xx} = \sum_{i=1}^{L-1} \sigma_i^x \sigma_{i+1}^x; \quad H_z = \sum_{i=1}^{L} \sigma_i^z; \quad H_{zz} = \sum_{i=1}^{L-1} \sigma_i^z \sigma_{i+1}^z. \tag{2}$$

In the above $\sigma_i^{x,y,z}$ are Pauli matrices on site i, g is the strength of transverse field, and $J_{x,z}$ is the strength of the Ising interaction in the x, z direction. We will set $J_x = 1$ in the following discussion. T qualitatively represents the period of the drive. In particular, taking $T \ll 1$ would recover the high-frequency limit where the Floquet Hamiltonian is simply $H_F = i(\ln U)/T = J_z H_{zz}/2 + gH_z/2 + H_{xx}/2$.

For J_z=0, the Floquet unitary becomes noninteracting, $U_0 = U|_{J_z=0}$, and the corresponding Floquet Hamiltonian $H_F^0 = i(\ln U_0)/T$ can be solved analytically for periodic boundary conditions. In particular (see Appendix A) we find

$$H_F^0 = \sum_{k>0} \epsilon_k (d_k^\dagger d_k - d_{-k} d_{-k}^\dagger), \tag{3}$$

where $d_k^\dagger (d_k)$ are the creation (annihilation) operators of Bogoliubov quasiparticles, and the bulk dispersion ϵ_k is

$$\cos(\epsilon_k T) = \cos(gT)\cos(J_x T) + \sin(gT)\sin(J_x T)\cos k. \tag{4}$$

The quasienergy band ϵ_k becomes exactly flat when either $J_x T = 0, \pi$ or $gT = 0, \pi$. The consequence of this on the decay rate of the edge modes will be emphasized later.

In contrast to continuous time, the quasienergy is only defined modulo $2\pi/T$, $\epsilon_k T \in [-\pi, \pi]$. Since within the Bogoliubov formalism, for each state with energy ϵ there has to be a state with energy $-\epsilon$, two values of ϵ, $\epsilon = 0$ and $\epsilon = \pi/T$ are special. This is because they have the property that $\epsilon T = -\epsilon T \mod 2\pi$, allowing for topologically protected modes at those energies. Therefore, two different types of edge modes, zero mode ψ_0 and π mode ψ_π can exist, with these modes appearing or disappearing via the gap closing at 0 or π. Depending on the choice of parameters, g and T, the system may possess none, one, or both of the two edge modes. When these edge modes exist, they anticommute with the Z_2 symmetry, $\mathcal{D} = \sigma_1^z \ldots \sigma_L^z$, of the system, $\{\psi_0, \mathcal{D}\} = \{\psi_\pi, \mathcal{D}\}$. In the thermodynamic limit of a semi-infinite chain, the zero and π modes respectively commute and anticommute with the Floquet unitary, $[\psi_0, U_0] = 0$, $\{\psi_\pi, U_0\} = 0$. Due to this property, they have infinite lifetime in the thermodynamic limit. Appendix B presents exact expressions for the 0 and π modes for the Floquet Ising model U_0.

When interactions are turned on, the commutation (anticommutation) relations between zero (π) mode and the Floquet unitary is violated. However, these edge modes are still long-lived quasistable modes, and are known as ASM. A useful quantity to probe this phenomena is the autocorrelation of σ_1^x,

$$A_\infty(n) = \frac{1}{2^L} \mathrm{Tr}\left[\sigma_1^x(n)\sigma_1^x\right], \tag{5}$$

where n is the stroboscopic time period. This is a good measure of the almost strong mode dynamics in the presence of interactions since both zero and π modes are localized on the edge with $\mathcal{O}(1)$ overlap with σ_1^x, $\mathrm{Tr}[\psi_0\sigma_1^x]/2^L \sim \mathcal{O}(1)$ and $\mathrm{Tr}[\psi_\pi\sigma_1^x]/2^L \sim \mathcal{O}(1)$. In the language of Majoranas, σ_1^x is the Majorana on the first site and the edge modes are a superposition of Majoranas, with largest weight being on the Majoranas near the boundary. We show an example of $A_\infty(n)$ in Fig. 1.

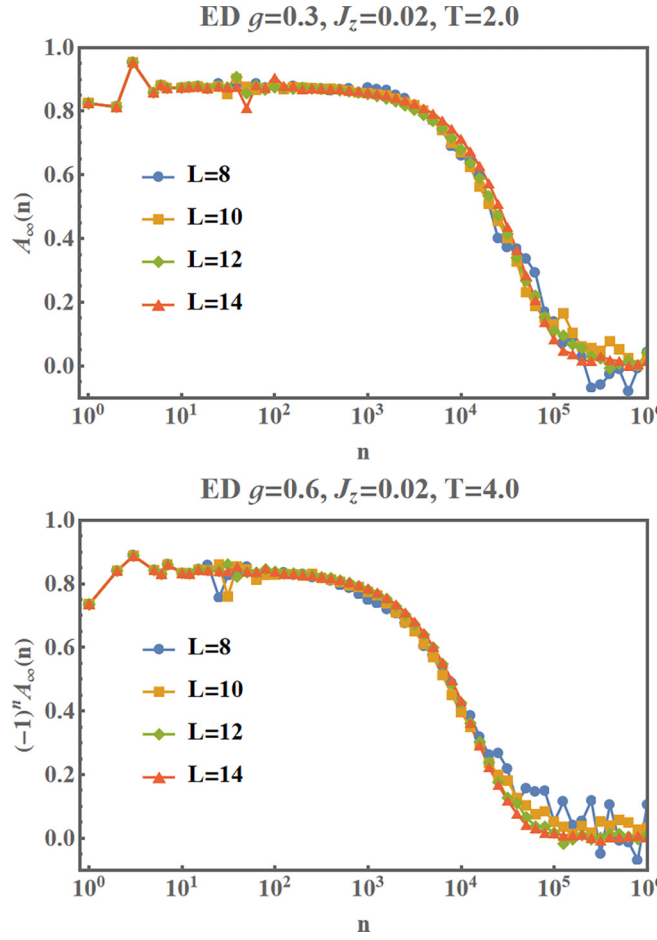

FIG. 1. The infinite temperature correlation A_∞ from exact diagonalization for different system sizes $L = 8, 10, 12, 14$. The plots show signatures of an almost strong zero mode (top panel) and an almost strong π mode (bottom panel) that survives for many cycles n before decaying. Note the different microscopic parameters g, T for the panels.

Figure 1 shows examples of ASMs. The top panel is for $g = 0.3, T = 2.0$ and shows an almost strong zero mode. The bottom panel is for a longer period $T = 4.0$ and a larger transverse field $g = 0.6$, and shows an almost strong π mode. Both panels are for the same strength of the integrability breaking term $J_z = 0.02$. After an initial transient, the autocorrelation

decays into a long-lived zero ψ_0 (upper panel) or ψ_π mode (lower panel) depending on the value of parameters g, T. The modes survive for many periods, indicated by the constant value of the autocorrelation function for the zero mode and the extra oscillation with the period $(-1)^n$ for the π mode. Eventually, the autocorrelations decay to zero due to interactions. Here the decay occurs around $\approx 10^4$ time cycles for both modes. Autocorrelation functions of bulk quantities (with no overlap with the ASMs) decay much faster, within 1–2 drive cycles.

For our model, the decay of ASMs can be captured by perturbation theory in the integrability breaking term. The interaction enables the scattering between the edge mode and bulk Majorana operators, with the leading contribution to the decay arising from resonance conditions, i.e., conditions that determine when the energy of the edge mode matches the total energy of certain number of bulk excitations, modulo $2\pi/T$. In the next section, we derive the decay rate of the infinite temperature autocorrelation function within second-order perturbation theory, i.e., $O(J_z^2)$, equivalently, FGR. Subsequently, we also discuss resonance conditions, which allow us to predict the leading power of J_z controlling the decay rates.

III. FGR AND BEYOND FOR INFINITE TEMPERATURE AUTOCORRELATION FUNCTION

Let us first examine the almost strong zero mode. In general, one can decompose the Floquet unitary into two parts,

$$U = e^{-iVT} e^{-iH_F^0 T}, \tag{6}$$

where V is the perturbation applied to the system and H_F^0 is the Floquet Hamiltonian of the unperturbed system. For the case we study in (1), one can identify the perturbation with $V = J_z H_{zz}/2$ and $H_F^0 = i(\ln U_0)/T$, where $U_0 = \exp(-iTgH_z/2)\exp(-iTJ_xH_{xx}/2)$. Performing a second-order expansion of V, the Floquet unitary is

$$U \approx \left(1 - iVT - \frac{V^2T^2}{2}\right) e^{-iH_F^0 T}. \tag{7}$$

After a period, the zero mode evolves into $\psi_0(1) = U^\dagger \psi_0 U$, and to second order in V, it is given by

$$\psi_0(1) \approx e^{i\mathcal{L}_0 T}\left(1 + iT\mathcal{L}_V + T^2\mathcal{G}_{V^2} - \frac{T^2}{2}\mathcal{F}_{V^2}\right)\psi_0. \tag{8}$$

In the above, we have used the notations $\mathcal{L}_0\psi_0 = [H_F^0, \psi_0]$, $\mathcal{L}_V\psi_0 = [V, \psi_0]$, $\mathcal{G}_{V^2}\psi_0 = V\psi_0 V$, and $\mathcal{F}_{V^2}\psi_0 = \{V^2, \psi_0\}$. Notice that $e^{i\mathcal{L}_0 T}\psi_0 = U_0^\dagger \psi_0 U_0 = \psi_0$ comes from the commutation relation between the zero mode and the unperturbed Floquet unitary.

After N periods we obtain (see Appendix C)

$$\psi_0(N) = \left[e^{i\mathcal{L}_0 T}\left(1 + iT\mathcal{L}_V + T^2\mathcal{G}_{V^2} - \frac{T^2}{2}\mathcal{F}_{V^2}\right)\right]^N \psi_0. \tag{9}$$

Now, we are in the position to calculate the autocorrelation of the zero mode

$$A_\infty^0(N) = \frac{1}{2^L}\mathrm{Tr}[\psi_0(N)\psi_0]. \tag{10}$$

By inserting (9) into the autocorrelation A_∞^0 and keeping terms up to second order in V, one arrives at

$$A_\infty^0(N) = A_\infty^0(0) - \frac{NT^2}{2^L}\left(\frac{1}{2}\mathrm{Tr}[\dot\psi_0\dot\psi_0] + \sum_{n\geqslant 1}^{\infty}\mathrm{Tr}[\dot\psi_0(n)\dot\psi_0]\right), \tag{11}$$

where we define $\dot\psi_0 = i\mathcal{L}_V\psi_0$, $\dot\psi_0(n) = e^{i\mathcal{L}_0 nT}\dot\psi_0$, and $A_\infty^0(0) = 1$ in our case.

The autocorrelation $A_\infty^0(N)$ with decay rate Γ_0 can be approximated by $A_\infty^0(N) \approx A_\infty^0(0)\exp(-NT\Gamma_0) \approx A_\infty^0(0)(1 - NT\Gamma_0)$ within perturbation theory. From this we conclude (see details in Appendix C) that the FGR decay rate for the zero mode correlation at second order in the perturbation, and in the large N limit is

$$\Gamma_0 = \frac{T}{A_\infty^0(0)2^L}\left(\frac{1}{2}\mathrm{Tr}[\dot\psi_0\dot\psi_0] + \sum_{n=1}^{\infty}\mathrm{Tr}[\dot\psi_0(n)\dot\psi_0]\right) = \frac{1}{A_\infty^0(0)2^L}\sum_{i,j}|\langle i|\tilde V|\tilde j\rangle|^2\pi\delta_F(\epsilon_i - \epsilon_j). \tag{12}$$

$|i\rangle$ are the many-particle eigenstates of the unperturbed unitary U_0 with eigenvalue $e^{-i\epsilon_i T}$. We define $\tilde V = V - \psi_0 V\psi_0$ and $|\tilde j\rangle = \psi_0|j\rangle$. Using $\psi_0^2 = 1$, one can rewrite $\tilde V = [V, \psi_0]\psi_0$, thus $\tilde V$ can be interpreted as the part of the interaction, which does not commute with the zero mode and thus changes it. In the above, the δ_F function encodes energy conservation modulo $2\pi/T$, with $\delta_F(\epsilon) = \sum_m \delta(\epsilon + m2\pi/T)$. In contrast to the traditional FGR for time-independent Hamiltonians, here one obtains quasienergy conservation, rather than energy conservation, due to the Floquet time evolution.

The FGR formula (12) has been derived from a short-time expansion, $NT\Gamma_0 \ll 1$, and it is therefore strictly speaking only valid if short and long-time behaviors are governed by the same decay process. This question has been studied in the context of the memory matrix formalism applied to integrable systems [26,27] and integrability breaking perturbations [28]. The analysis confirms that the perturbative formula is valid provided that the investigated mode is the slowest mode in the system: in this case short- and long-time decay coincide. This is justified for the almost strong modes studied in this paper.

For the π mode, the only difference comes from the anticommutation relation, $e^{i\mathcal{L}_0 T}\psi_\pi = U_0^\dagger\psi_\pi U_0 = -\psi_\pi$. It leads to extra factors of (-1) in the derivation. One can show (see Appendix C) that the π mode decay rate at second order in the perturbation is

$$\Gamma_\pi = \frac{T}{A_\infty^\pi(0)2^L}\left(\frac{1}{2}\mathrm{Tr}[\dot\psi_\pi\dot\psi_\pi] + \sum_{n=1}^{\infty}(-1)^n\mathrm{Tr}[\dot\psi_\pi(n)\dot\psi_\pi]\right) = \frac{1}{A_\infty^\pi(0)2^L}\sum_{i,j}|\langle i|\tilde V|\tilde j\rangle|^2\pi\delta_F\left(\epsilon_i - \epsilon_j + \frac{\pi}{T}\right). \tag{13}$$

In contrast to the zero mode, the $(-1)^n$ prefactor appears in the first line of (13), and is absorbed into the delta function by the inclusion of the π/T factor in the argument. The notation in the second line is slightly different from that for the zero mode, and is as follows: $\tilde V = V - \psi_\pi V\psi_\pi$ and $|\tilde j\rangle = \psi_\pi|j\rangle$.

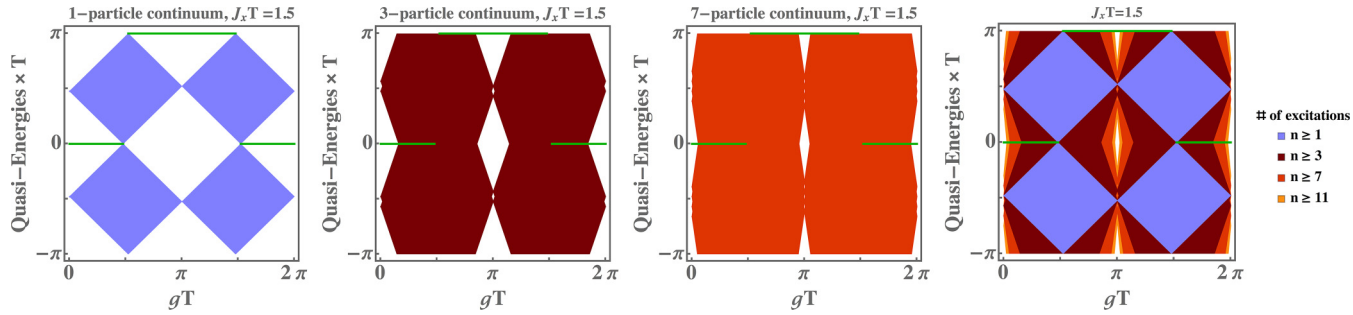

FIG. 2. Plot of quasienergies of n-particle excitations, $n = 1, 3, 7$, and a plot, where all these continua are combined, for $J_xT = 1.5$, and as a function of gT. See Appendix D for a description of how the continua are constructed. The thick dark green lines denote the position of the Majorana modes. The plot can be used to identify the dominant scattering process leading to a decay of the almost strong modes, see text.

The decay rates derived above for zero and π modes are only finite when the resonant conditions $\epsilon_i - \epsilon_j = 0$ and $\epsilon_i - \epsilon_j - \frac{\pi}{T} = 0$, respectively, are fulfilled (modulo $2\pi/T$). Our perturbation is $V = J_z H_{zz}/2$ and after a Jordan Wigner transformation, this can be written as a four Majorana fermion interaction term $\sigma_i^z \sigma_{i+1}^z = -a_{2i-1}a_{2i}a_{2i+1}a_{2i+2}$, where a_i are the Majorana operators. As a next step one can express those in terms of the edge-state Majorana ψ_0 and ψ_π and bulk operators d_k and $d_k^\dagger$. The matrix element $|\langle i|\tilde{V}|\tilde{j}\rangle|$ in FGR survives only when the perturbation V involves an edge mode such that $\tilde{V}$ is nonzero. To affect the edge mode, one of the operators has to be ψ_α with $\alpha = 0, \pi$, the others can be bulk modes. Thus in the thermodynamic limit a decay of ψ_0 in second-order perturbation theory is obtained if one finds a solution of the following equation:

$$0 = \epsilon_{k_1} \pm \epsilon_{k_2} \pm \epsilon_{k_3} \qquad (\mathrm{mod}\ 2\pi/T). \tag{14}$$

We therefore expect a nonzero decay rate of the ψ_0 mode at second order in J_z only if the three-particle continuum, defined by the sums and differences of three bulk energies ϵ_k, contains the energy 0. Figure 2 shows different n-particle continua as a function of gT and for a fixed value of $J_xT = 1.5$.

Similarly, the π mode will decay if one finds a solution for

$$\pi/T = \epsilon_{k_1} \pm \epsilon_{k_2} \pm \epsilon_{k_3} \qquad (\mathrm{mod}\ 2\pi/T). \tag{15}$$

Thus one has to check whether the three-particle continuum contains the quasienergy π/T. If both π and zero modes are present, scattering processes proportional to $\psi_0\psi_\pi$ and two bulk operators are possible, leading to the condition

$$\pi/T = \epsilon_{k_1} \pm \epsilon_{k_2} \qquad (\mathrm{mod}\ 2\pi/T). \tag{16}$$

This process is activated if the two-particle continuum includes the energy π/T. In this paper we discuss the decay of isolated $0, \pi$ modes, leaving the discussion of the decay when both modes are present to a later publication.

The conditions discussed above easily generalize to higher-order scattering processes. Matrix elements arising to order J_z^{2n} involve maximally $4n$ Majorana fermions and thus maximally $4n-1$ bulk modes. One therefore obtains a contribution to the decay rate of ψ_0 to order J_z^{2n} if a solution exists for

$$0 = \sum_{i=1}^{4n-1} (\pm\epsilon_{k_i}) \qquad (\mathrm{mod}\ 2\pi/T), \tag{17}$$

or, equivalently, if the energy 0 is part of the $(4n-1)$-particle continuum of the bulk states. The condition of (17) strongly restricts the phase space (i.e., the subset of allowed k_i values) available for scattering in a J_z^{2n}-scattering process. Similarly, the decay of the π mode is triggered for

$$\pi/T = \sum_{i=1}^{4n-1} (\pm\epsilon_{k_i}) \qquad (\mathrm{mod}\ 2\pi/T). \tag{18}$$

If both $0, \pi$ modes are present, there is a further decay channel arising from the $(4n-2)$-particle continuum,

$$\pi/T = \sum_{i=1}^{4n-2} (\pm\epsilon_{k_i}) \qquad (\mathrm{mod}\ 2\pi/T), \tag{19}$$

a regime we plan to explore in future work. The knowledge of the maxima and minima of the bulk dispersion ϵ_k of the integrable system are sufficient to construct analytically the m-particle continuum (see Appendix D). As shown in Fig. 2, the larger the number of excitations the larger is the range of quasienergies, which can couple to the modes.

Thus, without any further calculation, one can determine the leading power m in the decay rate, $\Gamma \sim J_z^m$, of the zero or π modes. For a given set of parameters, one has to determine the smallest value of n, which leads to a finite $4n-1$-particle continuum at either the quasienergy zero or π, see Fig. 2. This determines the exponent $m = 2n$ in the $J_z \to 0$ limit. This exponent is shown in Fig. 3, in the region where the edge modes exist, and accounting for m up to 8. For a large part of the phase diagram one obtains $\Gamma \sim J_z^2$, but there are also sizable regions in the phase diagram, where larger exponents are obtained, resulting in a much longer lifetime of the edge modes. The exponents m get larger and larger upon approaching the lines $gT = 0, \pi$ or $J_xT = 0, \pi$, which is explained by the fact that the quasiparticle bands become exactly flat in this limit, see (4). For such exactly flat bands, $\epsilon_k = \epsilon_c = \text{constant}$, one cannot find any solution for (17) and (18) [with the exception of points where $\epsilon_c/(2\pi/T)$ is a rational number]. Thus, the decay rate Γ of edge modes becomes smaller than any power law in this limit for $J_z \to 0$.

It is worth mentioning that the FGR formula is valid for any perturbation regardless of the symmetry. For example, a perturbation in the form of a y-direction transverse field breaks Z_2 symmetry. However, in second order, such a perturbation already involves many-Majorana scattering processes since σ_l^y

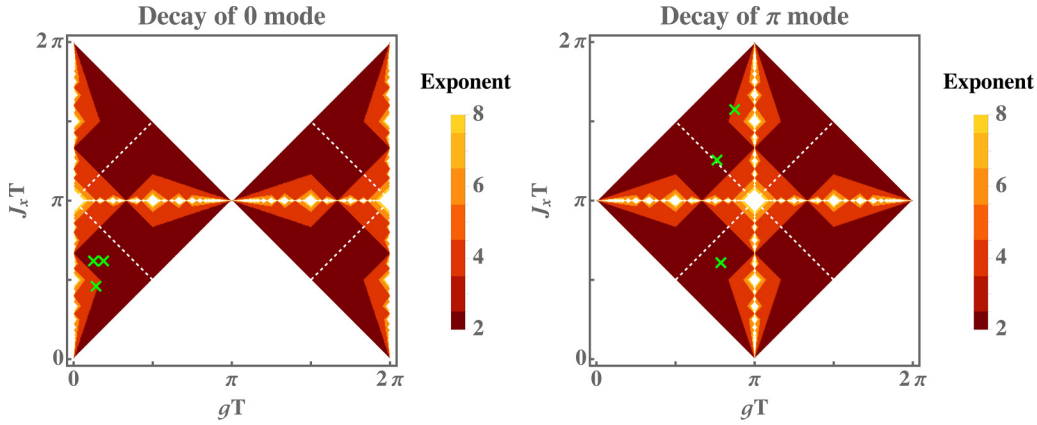

FIG. 3. Plot of the exponent m characterizing the decay of the zero mode (left panel) and the π mode (right panel) by bulk scattering processes. The decay rate is predicted to be proportional to J_z^m for $J_z \to 0$ where the exponent m is encoded in the color of the plot. The exponent $m = 2n$ is determined from the condition whether the energy of the mode is part of the $(4n-1)$-particle continuum, see Fig. 2 and text. Only those regions in parameter space are shown where the corresponding mode exists. The dashed white lines show the boundary of the existence for π mode (left panel) and 0 mode (right panel), and we focus on the region where only one kind of edge mode is allowed. The crosses denote parameter values investigated in Figs. 4 and 5.

is a string of Majoranas $\sigma_l^y = (-ia_1a_2)\ldots(-ia_{2l-3}a_{2l-2})a_{2l}$. Here we consider the Z_2-symmetric perturbation $V = J_z H_{zz}/2$ such that the perturbing term has only four Majoranas. This allows for a simpler physical picture for describing different decay channels.

In the following section, we present numerical results to support these ideas.

IV. RESULTS AND DISCUSSION

A. Almost strong zero mode

We first focus on the almost strong zero mode and how it is influenced by second-order processes. Two cases are studied, $g = 0.2, 0.3$ with $T = 2.0$ where the system possesses only a zero mode. They correspond to the top two crosses in the left panel of Fig. 3. The decay rate is dominated by second-order perturbation as the three-particle continuum is closed at zero quasienergy. The autocorrelation function of σ_1^x are computed from exact diagonalization, with the results for $L = 14$ presented in top panels (left and middle) of Fig. 4. The rescaled plots are shown in the corresponding bottom panels. The rescaled autocorrelation functions approach the FGR prediction for small J_z. In addition, the numerically fitted decay rates, shown for two different system sizes, are in agreement with the perturbative result (12), see inset of Fig. 4.

To go beyond the region where second-order perturbation theory is valid, we consider a shorter period $T = 1.5$ with $g = 0.3$. This corresponds to the lower single cross in the left panel of Fig. 3. Here, the system only possesses a zero mode but the resonance condition is satisfied by fourth-order perturbation instead of second-order perturbation theory. Notice that the third-order perturbation cannot be the leading order here because the decay rate is a positive number, and it should stay positive when $J_z \to -J_z$. Therefore, the leading-order contribution can only be an even-order perturbation.

The autocorrelation function and the numerically fitted decay rate are presented in the right panels of Fig. 4. As we are probing a higher-order perturbation process, the time scales for a given value of J_z become much longer, and finite system size effects and deviation from exponential behavior (see below) become more apparent in comparison to the second-order cases. In addition, the value of J_z cannot be taken to be as small as in the second-order region. The fitted decay rates and the plot of the autocorrelation functions as function of $J_z^4 n$ in the lower right panel of Fig. 4 clearly support a decay rate proportional to J_z^4 in the small J_z limit.

Deviations from simple exponential behavior appear both in regimes where the decay rates are proportional to J_z^2 and J_z^4. In the middle panel of Fig. 4, the autocorrelation function starts to clearly deviate from exponential decay for $J_z = 0.01$. Larger effects are seen in the right panel of Fig. 4, where decay rates are proportional to J_z^4. For all parameters where the curves do not follow a simple exponential decay in the long-time limit, we also observe finite-size effects as shown in Appendix E where numerical results for $L = 12$ and 14 are compared. Mathematically, deviations from exponential behavior at the long time scale nT, $n \gg 10^3$, reflects that the imaginary part of the self-energy of the Majorana mode depends on frequency in the small frequency scale $\sim 1/(nT)$. This arises because bulk quasienergies are discrete in a finite-size system. Nevertheless, as shown by the scaling plots, finite system size effects do not spoil the key features of the perturbative processes in the parameter region we have probed. Hence, the numerical results fully support the perturbative argument.

B. Almost strong π mode

Now, we turn to the decay of the π mode. We first focus on two different periods, $T = 4.0$ and $T = 8.25$, that allow the existence of a π mode for a range of g. We study two cases, $g = 0.6$, $T = 4.0$ and $g = 0.3$, $T = 8.25$ corresponding to the middle and bottom crosses in the right panel of Fig. 3. The decay is due to resonances that are second order in J_z. The autocorrelation function is presented in the top panels

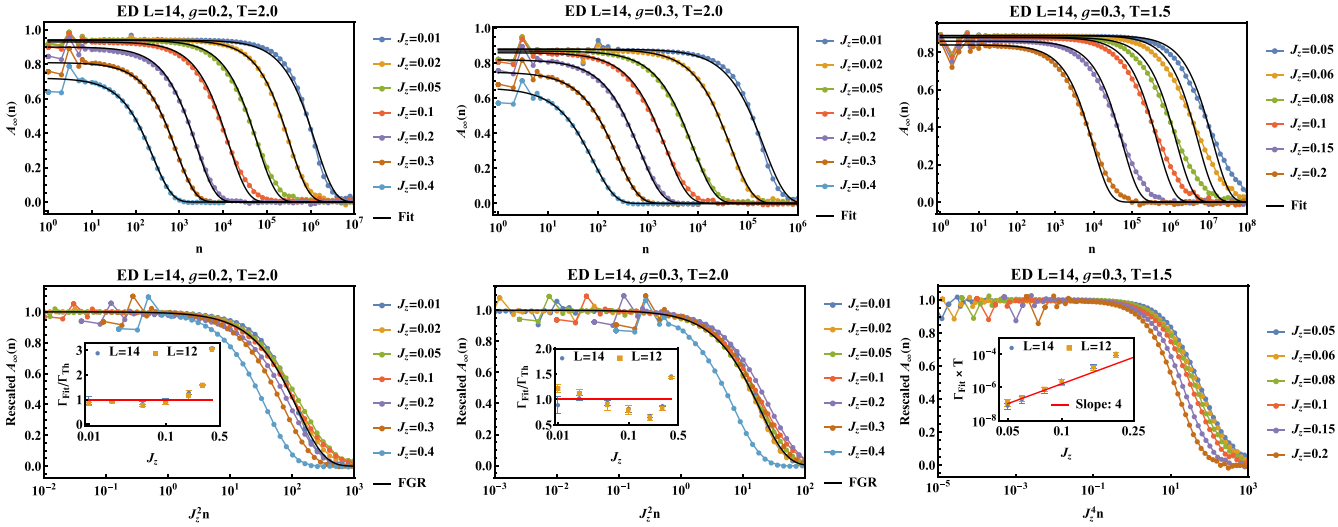

FIG. 4. Almost strong zero mode. Top panels: The infinite temperature autocorrelation of σ_1^x for $L = 14$ with $g = 0.2$, $T = 2.0$ (left), $g = 0.3$, $T = 2.0$ (middle) and $g = 0.3$, $T = 1.5$ (right) for different strengths of the integrability breaking term J_z. As J_z decreases, the lifetime increases. Each data set is fitted with an exponential function $C\exp(-NT\Gamma_{\rm fit})$ where the decay rate is determined from the average $\Gamma_{\rm fit} = (\Gamma_{80\%} + \Gamma_{20\%})/2$ where $\Gamma_{80\%(20\%)}$ is the inverse time at which the correlator is $0.8(0.2)C$. Bottom panels: The autocorrelation function is rescaled to be 1 in the quasistable region, and the time is rescaled to $J_z^2 n$ ($J_z^4 n$) for the second (fourth)-order perturbation process. For $g = 0.2$, $T = 2.0$ (left) and $g = 0.2$, $T = 3.0$ (middle), the rescaled autocorrelation function approaches the FGR theoretical values $\Gamma_{\rm Th}T$, which equals $0.0082J_z^2$ (left) and $0.054J_z^2$ (middle) for small J_z. The inset shows the ratio between the numerically fitted decay rate $\Gamma_{\rm Fit}$ and the theoretical decay rate $\Gamma_{\rm Th}$ for $L = 12, 14$. The horizontal red line marks $\Gamma_{\rm Fit}/\Gamma_{\rm Th} = 1$ and the error bar of each data point shows the range between $\Gamma_{80\%}$ and $\Gamma_{20\%}$. The numerical results validate second-order perturbation in J_z. For $g = 0.3$, $T = 1.5$ (right), the rescaled autocorrelation function and the inset that plots $\Gamma_{\rm Fit}T$ vs J_z on a log-log scale, are consistent with $\Gamma_{\rm Fit} \propto J_z^4$ for small J_z.

(left and middle) of Fig. 5. In the corresponding bottom panels in Fig. 5, the rescaled autocorrelation function is plotted and shown to approach the FGR prediction for small J_z. The numerically fitted decay rates are plotted in the corresponding insets of Fig. 5 and are shown to be consistent with the FGR result (13).

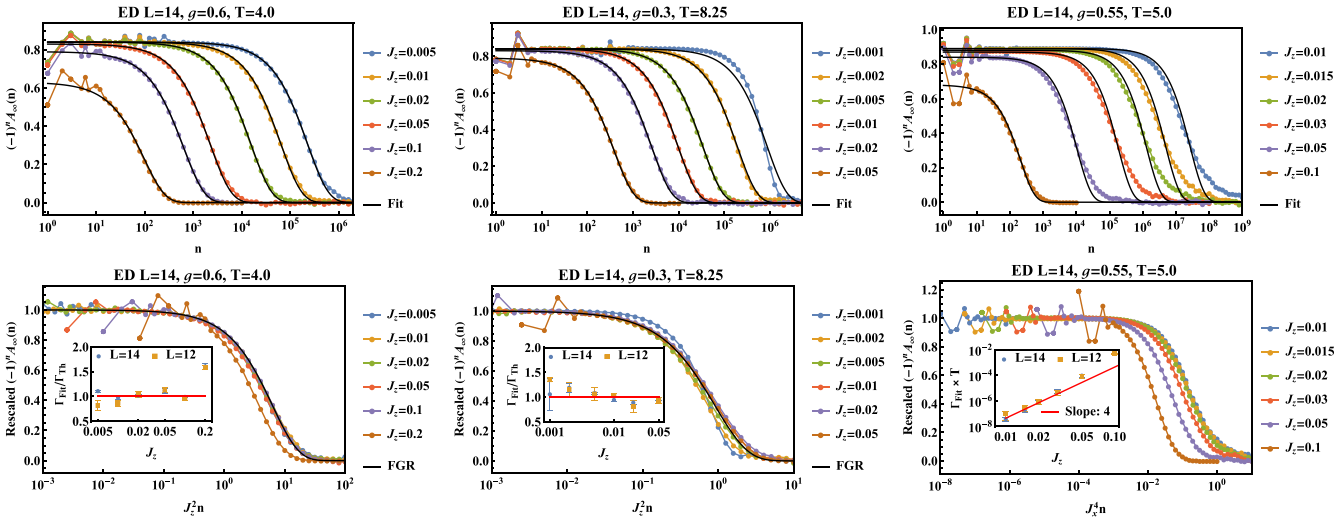

FIG. 5. Almost strong π mode. Top panels: The autocorrelation function of σ_1^x for $L = 14$ with $g = 0.6$, $T = 4.0$ (left), $g = 0.3$, $T = 8.25$ (middle) and $g = 0.55$, $T = 5.0$ (right) for different J_z. Here we multiply the autocorrelation function by $(-1)^n$ so that the time evolution is smooth, like a zero mode. In addition, we fit the time evolution to an exponential decay in the same manner as was done for the zero mode case discussed in Fig. 4. Bottom panels: The corresponding rescaled autocorrelation function vs rescaled time $J_z^2 n$ ($J_z^4 n$) for the second (fourth)-order perturbation process. For $g = 0.6$, $T = 4.0$ (left) and $g = 0.3$, $T = 8.25$ (middle), the rescaled autocorrelation function approaches the FGR theoretical values $\Gamma_{\rm Th}T$, which equal $0.16J_z^2$ (left) and $1.1J_z^2$ (middle) for small J_z. The inset shows the ratio between the numerically fitted decay rate $\Gamma_{\rm Fit}$ and the theoretical decay rate $\Gamma_{\rm Th}$ for $L = 12, 14$. The horizontal red line marks $\Gamma_{\rm Fit}/\Gamma_{\rm Th} = 1$ and the error bar of each data point shows the range between $\Gamma_{80\%}$ and $\Gamma_{20\%}$. The numerical results validate second-order perturbation in J_z. For $g = 0.3$, $T = 1.5$ (right), the rescaled autocorrelation function and the inset showing $\Gamma_{\rm Fit}T$ vs J_z on a log-log scale, are consistent with $\Gamma_{\rm Fit} \propto J_z^4$ for small J_z.

To explore resonances arising from higher-order processes, a different period $T = 5.0$ is considered with $g = 0.55$. This corresponds to the top cross in the right panel in Fig. 3, where the system only possesses a π mode but the resonance condition is matched by fourth-order perturbation theory instead of second-order perturbation theory. The autocorrelation function and the numerically fitted decay rate are presented in the right panels of Fig. 5. As with the zero mode case, the finite system size effect is apparent at $L = 14$ for higher-order processes, making the range of J_z that can be probed, more limited. Despite the deviation from exponential decay of the autocorrelation function, we can still estimate the decay rate by the same fitting method as before since the decay rates for $L = 12, 14$ overlap for J_z values as small as $J_z = 0.01$. The rescaled autocorrelation function plotted in the bottom right panel tends to saturate for small J_z. Qualitatively, the scaling of the decay rate shows a behavior consistent with J_z^4 for small J_z, in agreement with the resonance conditions deduced from studying the many-particle continuum.

The finite system size effects are visible in both second- and fourth-order dominated processes. When second-order processes are dominant, the finite system size effect is severe for $g = 0.3$, $T = 8.25$, for the small J_z value of $J_z = 0.001$ (middle panels). Here, the autocorrelation function deviates considerably from an exponential decay, and fails to collapse to the FGR prediction. This can also be observed in the increasing error bars in the fitted decay rate. On the contrary, the finite system size effect is not essential for $g = 0.6$, $T = 4.0$ (left panels) as the rescaled autocorrelation functions collapse well around the FGR prediction for small J_z. When fourth-order processes dominate (right panels), as with the zero mode case, the finite-size effects become more severe, with the autocorrelation functions following a slower decay than exponential for small J_z. A more detailed discussion of finite-size effects is presented in Appendix E.

Finally, we would like to stress the connection between this work and prethermalization [8,29]. If in a Floquet system the driving frequency ω is much larger than all other energy scales, then the heating rate, which drives the system to infinite temperature, is exponentially small [30,31]. Here, we investigate a somewhat different question: we assume that the system has already reached infinite temperature, and we explore under this condition, the stability of topological boundary modes. We are also not focusing on the limit where the frequency is much larger than the relevant bandwidth. Nevertheless, the physics, which leads to exponentially small decay rates is actually fully consistent with our approach. In Fig. 3, this is encoded in the fact that the exponent n gets larger and larger when one approaches parameters where the Floquet bands become flat ($J_x T = 0, \pi$ or $gT = 0, \pi$). A power-law decay rate $\Gamma \sim J_z^{2n} = e^{-2n \ln(1/J_z)}$ is equivalent to an exponential suppression (with logarithmic corrections), $\Gamma \sim e^{-c/W}$, provided that $n \propto 1/W$, where W is the bandwidth of the relevant band. Such a behavior follows from (17) and (18) when one considers first the limit of vanishing J_z and afterwards the limit of a vanishing bandwidth (the two limits do not commute).

To see this more clearly, note that for a decay rate $\propto J_z^{2n}$ of the zero mode, one needs to satisfy the following modulo 2π: $n_1 \epsilon_{\max} = n_2 \epsilon_{\min}$, $n_1 + n_2 = 4n - 1$ (see Appendix D). This implies $n_1 + n_2 = (n_2 - n_1)(\epsilon_{\max} + \epsilon_{\min})/(\epsilon_{\max} - \epsilon_{\min})$. Thus, in the limit of a narrow bandwidth $J_z \ll (\epsilon_{\max} - \epsilon_{\min})/(\epsilon_{\max} + \epsilon_{\min}) \ll 1$, we expect that the decay rate is approximately given by $J_z^{2n} \sim e^{-c/W}$, where $W = \epsilon_{\max} - \epsilon_{\min}$ and c depends logarithmically on J_z. This argument does not, however, take into account n-dependent combinatorial prefactors in the decay rate, which can lead to extra logarithmic corrections, see Refs. [30,31].

V. CONCLUSIONS

While periodically driven many-particle systems tend to heat up to infinite temperatures, almost strong modes can, nevertheless, have very long life times. Besides the size of integrability breaking terms, here the decisive factor is the phase space available for scattering. The conservation of quasienergies governs which states are available for scattering and thus controls in which order of perturbation theory one can obtain finite-decay rates. Our study tests this physics numerically in the perhaps most simple setting of a Floquet version of the one-dimensional Ising model, which can host two types of almost strong modes, zero and π modes. A major advantage of the model is that it can be simulated in a straightforward way on quantum computers [32], even if present-day devices are too noisy to explore the extremely long time scales relevant in our study.

Alternatively, our study can be viewed as an investigation of the stability of Majorana modes in static or periodically driven [33] one-dimensional topological superconductors with respect to quasiparticle poisoning. While nominally described by the same type of Hamiltonian, the edge modes in the superconducting realization are more stable with respect to noise, with a low-temperature environment strongly reducing scattering in comparison to our infinite-temperature calculation. In the Floquet case, the precise preparation protocol could also play a decisive role for the stability of the system [33]. Although we focus on a one-dimensional system in this paper, the Floquet FGR is generic and can be applied to study systems in higher dimension, e.g., two-dimensional higher-order Floquet topological superconductors [34,35].

To further explore the stability of almost strong modes and topological qubits, either in solid state realizations or in a quantum computer, it will be interesting to extend our study to noisy environments and to systems where phonons provide on the one hand cooling, and on the other hand novel quasiparticle poisoning channels.

ACKNOWLEDGMENTS

This work was primarily supported by the US Department of Energy, Office of Science, Basic Energy Sciences, under Award No. DE-SC0010821 (H.Y., A.M.) and by the German Research Foundation within CRC183 [Project No. 277101999, subproject A01 (A.R.) and partially by the Mercator Fellowship (A.M.)]. H.Y. acknowledges support of the NYU IT High Performance Computing resources, services, and staff expertise.

APPENDIX A: BULK DISPERSION RELATION IN FLOQUET TRANSVERSE-FIELD ISING MODEL

In this Appendix, we present a detailed derivation of the bulk dispersion of the Floquet transverse-field Ising model.

The same techniques can also be applied in the continuous time case. The Floquet unitary is

$$U_0 = U_z U_{xx}, \tag{A1}$$

where

$$U_z = \exp\left(-ig\frac{T}{2}H_z\right); \quad U_{xx} = \exp\left(-iJ_x\frac{T}{2}H_{xx}\right). \tag{A2}$$

H_z and H_{xx} are defined in (2) describing transverse field and Ising interactions respectively. The model can be mapped to a bilinear spinless Fermion model through the Jordan-Wigner transformation,

$$c_j^\dagger = \prod_{l<j}\sigma_l^z\sigma_j^-; \quad c_j = \prod_{l<j}\sigma_l^z\sigma_j^+, \tag{A3}$$

where $\sigma_j^\pm = (\sigma_j^x \pm i\sigma_j^y)/2$. Therefore, the spin interactions can be expressed in terms of c and $c^\dagger$ as follows:

$$\sigma_i^z = 1 - 2c_i^\dagger c_i, \tag{A4}$$

$$\sigma_i^x\sigma_{i+1}^x = c_i^\dagger c_{i+1}^\dagger + c_i^\dagger c_{i+1} + c_{i+1}^\dagger c_i + c_{i+1}c_i. \tag{A5}$$

We impose periodic boundary conditions and perform a Fourier transformation,

$$c_j = \frac{e^{i\pi/4}}{\sqrt{L}}\sum_k e^{ikj}c_k, \quad c_j^\dagger = \frac{e^{-i\pi/4}}{\sqrt{L}}\sum_k e^{-ikj}c_k^\dagger, \tag{A6}$$

where L is the system size. The spin Hamiltonians in k space are

$$H_z = \sum_{k>0}[c_k c_k^\dagger - c_k^\dagger c_k + c_{-k}c_{-k}^\dagger - c_{-k}^\dagger c_{-k}], \tag{A7}$$

$$H_{xx} = 2\sum_{k>0}[\cos k(c_k^\dagger c_k - c_{-k}c_{-k}^\dagger) + \sin k(c_k^\dagger c_{-k}^\dagger + c_{-k}c_k)]. \tag{A8}$$

The Floquet unitary can now be written as a product of unitaries in k space

$$U = \prod_{k>0} U_z^k U_{xx}^k, \tag{A9}$$

where

$$U_z^k = \exp\left[-i\frac{gT}{2}(c_k c_k^\dagger - c_k^\dagger c_k + c_{-k}c_{-k}^\dagger - c_{-k}^\dagger c_{-k})\right], \tag{A10}$$

$$U_{xx}^k = \exp[-iJ_xT(\cos k(c_k^\dagger c_k - c_{-k}c_{-k}^\dagger) + \sin k(c_k^\dagger c_{-k}^\dagger + c_{-k}c_k))]. \tag{A11}$$

It is useful to consider a 4×4 matrix representation of U_z^k and U_{xx}^k. We choose four orthogonal bases: $|0\rangle$, $|1\rangle = c_k^\dagger c_{-k}^\dagger|0\rangle$, $|2\rangle = c_k^\dagger|0\rangle$, and $|3\rangle = c_{-k}^\dagger|0\rangle$. In this basis U_z^k and U_{xx}^k are as follows:

$$U_z^k = \begin{pmatrix} \exp(-igT) & 0 & 0 & 0 \\ 0 & \exp(igT) & 0 & 0 \\ 0 & 0 & 1 & 0 \\ 0 & 0 & 0 & 1 \end{pmatrix}, \tag{A12}$$

$$U_{xx}^k = \begin{pmatrix} u_{xx} & 0_{2\times 2} \\ 0_{2\times 2} & \mathbb{I}_{2\times 2} \end{pmatrix}, \tag{A13}$$

where u_{xx} is a 2 by 2 matrix

$$u_{xx} = \mathbb{I}_{2\times 2}\cos(J_xT) - i\sin(J_xT)(\sigma_x\sin k - \sigma_z\cos k). \tag{A14}$$

Finally, the multiplication of these two matrices leads to

$$U_k = U_z^k U_{xx}^k = \begin{pmatrix} \alpha & \beta & 0 & 0 \\ -\beta^* & \alpha^* & 0 & 0 \\ 0 & 0 & 1 & 0 \\ 0 & 0 & 0 & 1 \end{pmatrix}, \tag{A15}$$

where

$$\alpha = e^{-igT}[\cos(J_xT) + i\sin(J_xT)\cos k], \tag{A16}$$

$$\beta = -ie^{-igT}\sin(J_xT)\sin k. \tag{A17}$$

Since $U_k U_k^\dagger = 1$, one obtains $|\alpha|^2 + |\beta|^2 = 1$. Focusing on the upper-left 2×2 block, the two eigenvalues $\exp(\pm i\epsilon_k T)$, are given by

$$\exp(\pm i\epsilon_k T) = \mathrm{Re}[\alpha] \pm i\sqrt{1 - \mathrm{Re}[\alpha]^2}. \tag{A18}$$

By examining the real part of (A18) with (A16), one arrives at

$$\cos(\epsilon_k T) = \cos(gT)\cos(J_xT) + \sin(gT)\sin(J_xT)\cos k. \tag{A19}$$

The above is the bulk dispersion reported in (4). Note that the quasienergy band ϵ_k becomes exactly flat when either $J_xT = 0, \pi$ or $gT = 0, \pi$.

The upper-left 2×2 block can be rewritten in an exponential form by employing $|\alpha|^2 + |\beta|^2 = 1$ and (A18),

$$\begin{pmatrix} \alpha & \beta \\ -\beta^* & \alpha^* \end{pmatrix} = \exp\left[-i\frac{\epsilon_k T}{\sqrt{1-\mathrm{Re}[\alpha]^2}}\begin{pmatrix} -\mathrm{Im}[\alpha] & i\beta \\ -i\beta^* & \mathrm{Im}[\alpha] \end{pmatrix}\right]. \tag{A20}$$

Accordingly, the Floquet Hamiltonian for a given k momentum is derived from $H_{F,k}^0 = i\ln(U_z^k U_{xx}^k)/T$. One obtains

$$H_{F,k}^0 = \frac{\epsilon_k}{\sqrt{1-\mathrm{Re}[\alpha]^2}}\begin{pmatrix} -\mathrm{Im}[\alpha] & i\beta & 0 & 0 \\ -i\beta^* & \mathrm{Im}[\alpha] & 0 & 0 \\ 0 & 0 & 0 & 0 \\ 0 & 0 & 0 & 0 \end{pmatrix}. \tag{A21}$$

Representing the above in terms of fermion bilinears, the full Floquet Hamiltonian is

$$H_F^0 = \sum_{k>0}\frac{\epsilon_k}{\sqrt{1-\mathrm{Re}[\alpha]^2}}(c_k^\dagger \quad c_{-k})\begin{pmatrix} \mathrm{Im}[\alpha] & -i\beta^* \\ i\beta & -\mathrm{Im}[\alpha] \end{pmatrix}\begin{pmatrix} c_k \\ c_{-k}^\dagger \end{pmatrix}. \tag{A22}$$

Diagonalizing the above via a Bogoliubov transformation leads to the Floquet Hamiltonian (3),

$$H_F^0 = \sum_{k>0}\epsilon_k(d_k^\dagger \quad d_{-k})\begin{pmatrix} 1 & 0 \\ 0 & -1 \end{pmatrix}\begin{pmatrix} d_k \\ d_{-k}^\dagger \end{pmatrix}, \tag{A23}$$

where $(d_k^\dagger\ d_{-k}) = (c_k^\dagger\ c_{-k})S$ with the transformation matrix S given by

$$S = \begin{pmatrix} \frac{\sqrt{1-\mathrm{Re}[\alpha]^2}+\mathrm{Im}[\alpha]}{\sqrt{(\sqrt{1-\mathrm{Re}[\alpha]^2}+\mathrm{Im}[\alpha])^2+|\beta|^2}} & \frac{i\beta^*}{\sqrt{(\sqrt{1-\mathrm{Re}[\alpha]^2}+\mathrm{Im}[\alpha])^2+|\beta|^2}} \\ \frac{i\beta}{\sqrt{(\sqrt{1-\mathrm{Re}[\alpha]^2}+\mathrm{Im}[\alpha])^2+|\beta|^2}} & \frac{\sqrt{1-\mathrm{Re}[\alpha]^2}+\mathrm{Im}[\alpha]}{\sqrt{(\sqrt{1-\mathrm{Re}[\alpha]^2}+\mathrm{Im}[\alpha])^2+|\beta|^2}} \end{pmatrix}. \tag{A24}$$

APPENDIX B: ZERO MODE AND π MODE IN FLOQUET TRANSVERSE-FIELD ISING MODEL

In this Appendix, we present analytic expressions for the zero and π modes of the Floquet transverse-field Ising model. First, we introduce Majorana operators on odd and even sites following the convention that l runs over 1 to system size L,

$$a_{2l-1} = \prod_{j=1}^{l-1}\sigma_j^z\sigma_l^x; \quad a_{2l} = \prod_{j=1}^{l-1}\sigma_j^z\sigma_l^y. \tag{B1}$$

Next, we construct a generic operator as a linear combination of single Majorana operators, $\psi = \sum_n c_n a_n$. After one period of time evolution, the operator is still a superposition of single Majoranas

$$U_0^\dagger \psi U_0 = K\psi, \tag{B2}$$

where ψ is $(c_0\ c_1 \cdots)^T$, a column vector representation of $\psi = \sum_n c_n a_n$. The corresponding K in the same representation is

$$K = \begin{pmatrix} c_g & s_g & & & & & \\ -s_g c_{J_x} & c_g c_{J_x} & c_g s_{J_x} & s_g s_{J_x} & & & \\ s_g s_{Jx} & -c_g s_{J_x} & c_g c_{J_x} & s_g c_{J_x} & & & \\ & & -s_g c_{J_x} & c_g c_{J_x} & c_g s_{J_x} & s_g s_{J_x} & \\ & & s_g s_{Jx} & -c_g s_{J_x} & c_g c_{J_x} & s_g c_{J_x} & \\ & & & & & & \ddots \end{pmatrix}. \tag{B3}$$

Above, we use the shorthand notation: $c_g = \cos(gT)$, $s_g = \sin(gT)$, $c_{J_x} = \cos(J_x T)$, and $s_{J_x} = \sin(J_x T)$. The zero and π modes satisfy the eigenvalue equation

$$K\psi_0 = \psi_0; \quad K\psi_\pi = -\psi_\pi, \tag{B4}$$

which guarantees commutation and anticommutation relations with the Floquet unitary. Here, we simply write down the answer, which can be checked by direct substitution into (B4),

$$\psi_0 \propto \sum_{l=1}\left\{\left[\cos\left(\frac{gT}{2}\right)a_{2l-1} + \sin\left(\frac{gT}{2}\right)a_{2l}\right] \times \left[\tan\left(\frac{gT}{2}\right)\cot\left(\frac{J_x T}{2}\right)\right]^{l-1}\right\}, \tag{B5}$$

$$\psi_\pi \propto \sum_{l=1}\left\{\left[\sin\left(\frac{gT}{2}\right)a_{2l-1} - \cos\left(\frac{gT}{2}\right)a_{2l}\right] \times \left[-\cot\left(\frac{gT}{2}\right)\cot\left(\frac{J_x T}{2}\right)\right]^{l-1}\right\}. \tag{B6}$$

When applying FGR (12) and (13), we numerically construct the normalized zero and π modes according to the analytic expressions (B5) and (B6). Note that the commutation and anticommutation relations only hold in the thermodynamic limit. However, the analytic solutions are localized on the edge with commutation and anticommutation relations spoiled by a number, which is exponentially small in the system size. Hence, one can still apply FGR with a finite system size truncation of (B5) and (B6).

APPENDIX C: FGR FOR THE DECAY OF THE INFINITE TEMPERATURE AUTOCORRELATION

In this Appendix, we provide the full derivation of the FGR decay rate of the infinite temperature autocorrelation of almost strong zero and π modes. The full Floquet unitary consists of two parts: one arising from a perturbing interaction V and the other arising from the unperturbed Floquet Hamiltonian H_F^0,

$$U = e^{-iVT}e^{-iH_F^0 T}. \tag{C1}$$

To second order in V, one obtains

$$U \approx \left(1 - iVT - \frac{V^2T^2}{2}\right)e^{-iH_F^0 T}. \tag{C2}$$

Now, we consider the time evolution of the zero and π modes after one period, $U^\dagger\psi_\eta U$ with $\eta = 0$ or π for zero and π modes respectively. Up to second order

$$\psi_\eta(1) = e^{i\mathcal{L}_0 T}\left(1 + iT\mathcal{L}_V + T^2\mathcal{G}_{V^2} - \frac{T^2}{2}\mathcal{F}_{V^2}\right)\psi_\eta. \tag{C3}$$

The notations are as follows: $\mathcal{L}_0\psi_\eta = [H_F^0, \psi_\eta]$, $\mathcal{L}_V\psi_\eta = [V, \psi_\eta]$, $\mathcal{G}_{V^2}\psi_\eta = V\psi_\eta V$, and $\mathcal{F}_{V^2}\psi_\eta = \{V^2, \psi_\eta\}$. After N periods

$$\psi_\eta(N) = \left[e^{i\mathcal{L}_0 T}\left(1 + iT\mathcal{L}_V + T^2\mathcal{G}_{V^2} - \frac{T^2}{2}\mathcal{F}_{V^2}\right)\right]^N\psi_\eta. \tag{C4}$$

The infinite temperature autocorrelation is given by

$$A_\infty^\eta(N) = \frac{1}{2^L}\mathrm{Tr}[\psi_\eta(N)\psi_\eta]. \tag{C5}$$

We will only expand up to second order in V and denote $A_{\infty,n}^\eta$ to be the autocorrelation function to nth order in V. At the zeroth order, one does not pick up any terms containing V, so that

$$A_{\infty,0}^\eta(N) = \frac{1}{2^L}\mathrm{Tr}\left[\left\{e^{i\mathcal{L}_0 TN}\psi_\eta\right\}\psi_\eta\right] = e^{i\eta N}, \tag{C6}$$

where we have applied the commutation relation $e^{i\mathcal{L}_0 T}\psi_\eta = e^{i\eta}\psi_\eta$ and employed the normalization $\mathrm{Tr}[\psi_\eta\psi_\eta]/2^L = 1$.

At first order, $\mathcal{L}_V$ appears once in the expansion

$$A_{\infty,1}^\eta(N) = \frac{1}{2^L}\sum_{n=0}^{N-1}\mathrm{Tr}\left[\left\{e^{i\mathcal{L}_0 T(N-n)}(iT\mathcal{L}_V)e^{i\mathcal{L}_0 Tn}\psi_\eta\right\}\psi_\eta\right]. \tag{C7}$$

With cyclic permutation within the trace, one can show that $\mathrm{Tr}[\{e^{i\mathcal{L}_0 T}O_1\}O_2] = \mathrm{Tr}[O_1\{e^{-i\mathcal{L}_0 T}O_2\}]$ for arbitrary operators

O_1 and O_2. Also, from the commutation relations, the first-order expansion is further simplified as

$$A^{\eta}_{\infty,1}(N) = \frac{e^{i\eta N}}{2^L}\sum_{n=0}^{N-1}\mathrm{Tr}[\{(iT\mathcal{L}_V)\psi_\eta\}\psi_\eta] = 0. \tag{C8}$$

Note that we have used $e^{i\eta} = e^{-i\eta}$ $(e^{2i\eta} = 1)$ since we only consider $\eta = 0$ or π. The above quantity is traceless due to the cyclic property of the trace: $\mathrm{Tr}[\{\mathcal{L}_V\psi_\eta\}\psi_\eta] = \mathrm{Tr}[\psi_\eta\{-\mathcal{L}_V\psi_\eta\}] = 0$.

Last, at second order, one has $\mathcal{G}_{V^2}$ once, $\mathcal{F}_{V^2}$ once or $\mathcal{L}_V$ twice in the expansion,

$$\begin{aligned}A^{\eta}_{\infty,2}(N) = {}& \frac{1}{2^L}\sum_{n=0}^{N-1}\mathrm{Tr}\Big[\Big\{e^{i\mathcal{L}_0T(N-n)}(T^2\mathcal{G}_{V^2})e^{i\mathcal{L}_0Tn}\psi_\eta\Big\}\psi_\eta\Big]\\ &- \frac{1}{2^L}\sum_{n=0}^{N-1}\mathrm{Tr}\left[\left\{e^{i\mathcal{L}_0T(N-n)}\left(\frac{T^2}{2}\mathcal{F}_{V^2}\right)e^{i\mathcal{L}_0Tn}\psi_\eta\right\}\psi_\eta\right]\\ &+ \frac{1}{2^L}\sum_{n\geqslant 1,m\geqslant 0}^{n+m=N-1}\mathrm{Tr}\Big[\Big\{e^{i\mathcal{L}_0T(N-n-m)}(iT\mathcal{L}_V)e^{i\mathcal{L}_0Tn}\\ &\times(iT\mathcal{L}_V)e^{i\mathcal{L}_0Tm}\psi_\eta\Big\}\psi_\eta\Big].\end{aligned} \tag{C9}$$

In the first and second trace, one obtains an overall factor $e^{i\eta N}$. Moreover, $\mathrm{Tr}[\{\mathcal{G}_{V^2}\psi_\eta\}\psi_\eta] = \mathrm{Tr}[V\psi_\eta V\psi_\eta]$ and $\mathrm{Tr}[\{\mathcal{F}_{V^2}\psi_\eta\}\psi_\eta] = 2\mathrm{Tr}[\psi_\eta VV\psi_\eta]$. Combining them and summing over n leads to a simple form

$$\begin{aligned}&\frac{1}{2^L}\sum_{n=0}^{N-1}\mathrm{Tr}\Big[\Big\{e^{i\mathcal{L}_0T(N-n)}(T^2\mathcal{G}_{V^2})e^{i\mathcal{L}_0Tn}\psi_\eta\Big\}\psi_\eta\Big]\\ &\quad- \frac{1}{2^L}\sum_{n=0}^{N-1}\mathrm{Tr}\left[\left\{e^{i\mathcal{L}_0T(N-n)}\left(\frac{T^2}{2}\mathcal{F}_{V^2}\right)e^{i\mathcal{L}_0Tn}\psi_\eta\right\}\psi_\eta\right]\\ &= -\frac{e^{i\eta N}NT^2}{2}\times\frac{1}{2^L}\mathrm{Tr}[\dot\psi_\eta\dot\psi_\eta],\end{aligned} \tag{C10}$$

where we define $\dot\psi_\eta = i\mathcal{L}_V\psi_\eta$. Now the last piece is the term with $\mathcal{L}_V$ in (C9). As we have learnt from the first-order expansion, $e^{i\mathcal{L}_0T(N-n-m)}$ and $e^{i\mathcal{L}_0Tm}$ contribute an overall factor $e^{i\eta(N-n)}$. Then, one associates the first $i\mathcal{L}_V$ with the last ψ_η by cyclic permutation. After summing over m, one obtains

$$\begin{aligned}&\frac{1}{2^L}\sum_{n\geqslant 1,m\geqslant 0}^{n+m=N-1}\mathrm{Tr}\Big[\Big\{e^{i\mathcal{L}_0T(N-n-m)}(iT\mathcal{L}_V)e^{i\mathcal{L}_0Tn}\\ &\quad\times(iT\mathcal{L}_V)e^{i\mathcal{L}_0Tm}\psi_\eta\Big\}\psi_\eta\Big]\\ &= -\frac{NT^2}{2^L}\sum_{n\geqslant 1}^{N}e^{i\eta(N-n)}\Big(1-\frac{n}{N}\Big)\mathrm{Tr}\big[\dot\psi_\eta(n)\dot\psi_\eta\big],\end{aligned} \tag{C11}$$

where we define $\dot\psi_\eta(n) = e^{i\mathcal{L}_0Tn}\dot\psi_\eta$.

On combining the above results, the autocorrelation function up to second order in V is

$$A^{\eta}_{\infty}(N) \approx A^{\eta}_{\infty,0}(N) + A^{\eta}_{\infty,2}(N), \tag{C12}$$

where

$$A^{\eta}_{\infty,0}(N) = e^{i\eta N} \tag{C13}$$

$$A^{\eta}_{\infty,2}(N) = -\frac{e^{i\eta N}NT^2}{2^L}\left(\frac{1}{2}\mathrm{Tr}[\dot\psi_\eta\dot\psi_\eta] + \sum_{n\geqslant 1}^{\infty}e^{i\eta n}\mathrm{Tr}[\dot\psi_\eta(n)\dot\psi_\eta]\right). \tag{C14}$$

Note that we approximate the upper bound of the summation N by ∞, and therefore the $(1 - n/N)$ in the summation is replaced by 1. Since we study quantities where the lifetime is long, N is chosen to be a large number. In addition, $\mathrm{Tr}[\dot\psi_\eta(n)\dot\psi_\eta]$ decays fast with a time scale much smaller than N. Therefore, we can simply replace N by ∞ in the summation.

The autocorrelation function with decay rate Γ_η can be formulated as $A^{\eta}_{\infty}(N) = e^{i\eta N}e^{-\Gamma_\eta NT} \approx e^{i\eta N}(1 - \Gamma_\eta NT)$. By comparing this to the second-order expansion, we obtain the FGR decay rate

$$\Gamma_\eta = \frac{T}{2^L}\left(\frac{1}{2}\mathrm{Tr}[\dot\psi_\eta\dot\psi_\eta] + \sum_{n=1}^{\infty}e^{i\eta n}\mathrm{Tr}[\dot\psi_\eta(n)\dot\psi_\eta]\right), \tag{C15}$$

which is the first line in (12) for $\eta = 0$ and (13) for $\eta = \pi$. One can reformulate the terms in the round parenthesis as

$$\begin{aligned}&\frac{1}{2}\mathrm{Tr}[\dot\psi_\eta\dot\psi_\eta] + \sum_{n\geqslant 1}^{\infty}e^{i\eta n}\mathrm{Tr}[\dot\psi_\eta(n)\dot\psi_\eta]\\ &\quad= \sum_{i,j}|\langle i|\dot\psi_\eta|j\rangle|^2\left(\frac{1}{2} + \sum_{n=1}^{\infty}e^{i(\epsilon_iT-\epsilon_jT+\eta)n}\right),\end{aligned} \tag{C16}$$

where $|i\rangle$ and $|j\rangle$ are eigenbases of U_0. The relation between Dirac delta function and summation of exponential is given by

$$\sum_{m=-\infty}^{\infty}2\pi\delta(x+2\pi m) = \sum_{n=-\infty}^{\infty}e^{ixn} = 2\left(\frac{1}{2} + \sum_{n=1}^{\infty}e^{ixn}\right). \tag{C17}$$

Therefore, the FGR decay rate can be expressed as

$$\Gamma_\eta = \frac{1}{2^L}\sum_{i,j}|\langle i|\dot\psi_\eta|j\rangle|^2\pi\delta_F\left(\epsilon_i - \epsilon_j + \frac{\eta}{T}\right), \tag{C18}$$

where $\delta_F(\epsilon) = \sum_m\delta(\epsilon + m2\pi/T)$ is the δ-function encoding energy conservation modulo $2\pi/T$. The matrix element can be further recast as

$$|\langle i|\dot\psi_\eta|j\rangle| = |\langle i|(V - \psi_\eta V\psi_\eta)\psi_\eta|j\rangle| = |\langle i|\tilde V|\tilde j\rangle|, \tag{C19}$$

where we use $\psi_\eta^2 = 1$ and define $|\tilde j\rangle = \psi_\eta|j\rangle$ and $\tilde V = V - \psi_\eta V\psi_\eta$. Finally, we arrive at the results in the second lines of (12) and (13),

$$\Gamma_\eta = \frac{1}{2^L}\sum_{i,j}|\langle i|\tilde V|\tilde j\rangle|^2\pi\delta_F\left(\epsilon_i - \epsilon_j + \frac{\eta}{T}\right). \tag{C20}$$

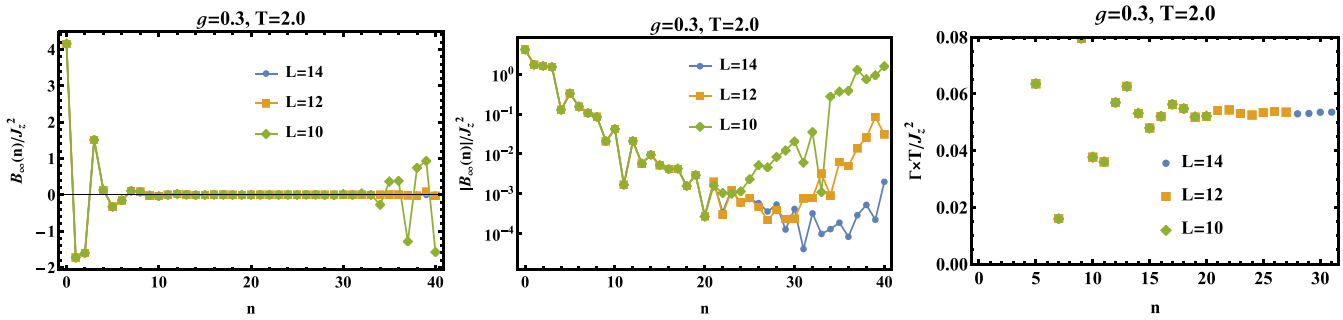

FIG. 6. The infinite temperature autocorrelation of $\dot{\psi}_0$, $B_n = \mathrm{Tr}[\dot{\psi}_0(n)\dot{\psi}_0]/2^L$ (left and middle) and the decay rate (right). J_z is the perturbation strength and the results are J_z independent on multiplying by $1/J_z^2$. The left panel shows a fast decay that supports the approximation in (C14). The fluctuation becomes large at later times for $L = 10$, which is the revival effect of a finite-size system. This can be clearly seen in the middle panel, where the revivals occur later as the system size increases. To take finite system size into account, we truncate the summation of n in (C15) up to the minimum value in the middle plot. In the right panel, we show how the decay rate converges as the upper bound of the summation (denoted by n on the x axis) increases.

In Fig. 6 we use the zero mode as an example to demonstrate the numerical computation of the infinite temperature autocorrelation $B_\infty(n) = \mathrm{Tr}[\dot{\psi}_0(n)\dot{\psi}_0]/2^L$, and the decay rate derived from it based on (12).

APPENDIX D: MANY PARTICLE QUASI-ENERGY CONTINUUM

In this Appendix, we illustrate how to numerically construct the manyparticle quasienergy continuum. For fixed parameters J_x, g, T, the bulk quasienergy spectrum $\epsilon_k T$ is a continuum within the interval $[\epsilon_{\min}T, \epsilon_{\max}T]$, where $\epsilon_{\min} = \min\{\epsilon_0, \epsilon_\pi\}$ and $\epsilon_{\max} = \max\{\epsilon_0, \epsilon_\pi\}$, where ϵ_k is given in (4). In this paper, the perturbation we consider is $J_z \sum_i \sigma_i^z \sigma_{i+1}^z = -J_z \sum_i a_{2i-1}a_{2i}a_{2i+1}a_{2i+2}$, i.e., a four Majorana interaction term. In the language of Feynman diagrams, the decay rate comes from the self-energy diagram obtained from contracting say n number of four Majorana interaction terms with two external lines left out. At $2n$-th order, there are $4n-1$ internal lines. The resonance condition is numerically determined by constructing the $4n-1$ particle quasienergy continuum from the bulk dispersion.

Let us start with the one-particle continuum. Each internal line can represent either the creation or annihilation of a quasiparticle because a Majorana is a linear combination of the creation and annihilation operator of a complex fermion (or Bogoliubov particle). The one-particle continuum is therefore $[\epsilon_{\min}T, \epsilon_{\max}T] \cup [-\epsilon_{\max}T, -\epsilon_{\max}T]$. For $n = 1$, we have to consider the three-particle continuum. The possible combinations are: create (annihilate) three quasiparticles, create (annihilate) two quasiparticles and annihilate (create) one quasiparticle. The three-quasiparticle continuum is therefore $[3\epsilon_{\min}T, 3\epsilon_{\max}T] \cup [-3\epsilon_{\max}T, -3\epsilon_{\max}T] \cup [(2\epsilon_{\min} - \epsilon_{\max})T, (2\epsilon_{\max} - \epsilon_{\min})T] \cup [(\epsilon_{\min} - 2\epsilon_{\max})T, (\epsilon_{\max} - 2\epsilon_{\min})T]$. For larger n, the construction is similar, and we do not show it here.

Once all the energy continuum are constructed, one has to fold them into the window $[-\pi, \pi]$ since quasienergies are only defined modulo 2π. For a given continuum, $[a, b]$, we shift it into the $[-\pi, \pi]$ interval as follows. First we shift

$$[a, b] \to [a', b'], \tag{D1}$$

where

$$a' = a - 2\pi \left\lfloor \frac{a+\pi}{2\pi} \right\rfloor, \tag{D2}$$

$$b' = b - 2\pi \left\lfloor \frac{a+\pi}{2\pi} \right\rfloor, \tag{D3}$$

with the floor function $\lfloor\ \rfloor$. Based on the three possible conditions we further fold $[a', b']$ into the $[-\pi, \pi]$ interval in the following different manners.

If $b' - a' > 2\pi$,

$$[a', b'] \to [-\pi, \pi]. \tag{D4}$$

If $b' > \pi$ and $b' - a' < 2\pi$

$$[a', b'] \to [a', \pi] \cup [-\pi, b' - 2\pi]. \tag{D5}$$

If $b' < \pi$ and $b' - a' < 2\pi$,

$$[a', b'] \to [a', b']. \tag{D6}$$

These three conditions cover all possible cases for a given interval $[a', b']$.

APPENDIX E: FINITE SYSTEM SIZE EFFECTS IN NUMERICAL RESULTS

In numerical computations, we obtain the autocorrelation functions in the thermodynamic limit by increasing the system size until the results saturate. In Fig. 7 we show a comparison of the decay of the almost strong modes for two different system sizes, $L = 12$ and $L = 14$. In the second-order region (left and middle panels of Fig. 7), the finite system size effects arise in the tails, in particular, $L = 12$ shows a slower decay at late times.

The perfect exponential decay comes from the fact that the energy spectrum is continuous in the thermodynamic limit and hence the delta function condition is obeyed in the FGR formula. However, for finite system sizes, the discrete energy spectrum will be detected at time scales long as compared to the inverse of the energy spacing of the multiparticle excitations. In bare perturbation theory to order J_z^{2n}, the relevant level spacing is proportional to $1/L^{4n-1}$. Due to the $4n-1$ bulk energies involved in the scattering process, there are

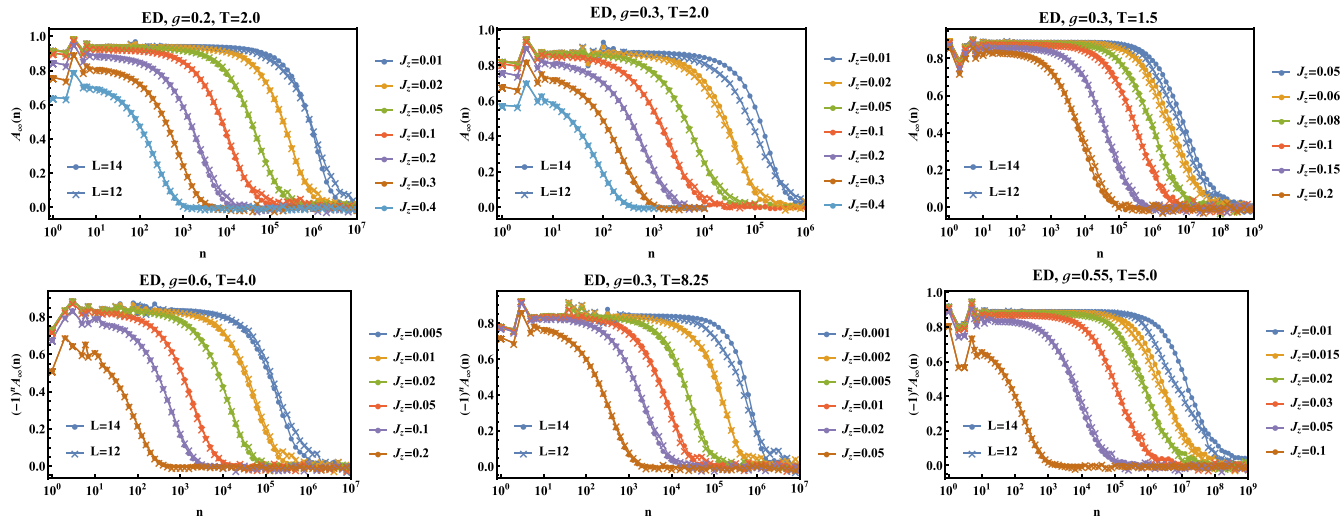

FIG. 7. Top panels: Almost strong zero mode. Bottom panels: Almost strong π mode. Comparison between the infinite temperature autocorrelation functions for $L = 12, 14$. The parameters g, T, J_z are chosen to be the same as Figs. 4 and 5. For second-order perturbation (left and middle panels), $L = 12$ shows a slowly decaying tail, which is a finite system size effect. $L = 14$ also shows finite system size effects, which manifest as a deviation from saturation from the thermodynamic limit (nonoverlapping of $L = 12, 14$ plots) for $n \gtrsim 10^6$. For fourth-order processes (right panels), the life times for small J_z are longer than $n = 10^6$. At these times, the system size effect is already strong for $L = 14$.

$O(L^{4n-1})$ multiparticle energies $\sum_{i=1}^{4n-1}(\pm\epsilon_{k_i})$ entering, e.g., in (17) or (18). Thus, finite-size effects are expected when the decay rate $\Gamma \sim W(J_z/W)^{2n}$ becomes smaller than W/L^{4n-1} where W is the relevant quasiparticle bandwidth. Thus finite-size effects are expected for $J_z \lesssim W/L^{3/2}$ for $n = 1$ (left and middle panels of Fig. 7) and for $J_z \lesssim W/L^{7/4}$ for $n = 2$ (right panels of Fig. 7). This is roughly consistent with our numerical results. Note that the estimate above does not take into account that bulk scattering leads to a finite lifetime of bulk modes, which can further suppress finite-size effects because the many-particle level spacing is exponentially small in L [36].

[1] T. Oka and S. Kitamura, Floquet engineering of quantum materials, Annu. Rev. Condens. Matter Phys. **10**, 387 (2019).

[2] F. Harper, R. Roy, M. S. Rudner, and S. Sondhi, Topology and broken symmetry in Floquet systems, Annu. Rev. Condens. Matter Phys. **11**, 345 (2020).

[3] A. Y. Kitaev, Unpaired Majorana fermions in quantum wires, Phys.-Usp. **44**, 131 (2001).

[4] P. Fendley, Parafermionic edge zero modes in Zn-invariant spin chains, J. Stat. Mech.: Theory Exp. (2012) P11020.

[5] P. Fendley, Strong zero modes and eigenstate phase transitions in the XYZ/interacting Majorana chain, J. Phys. A: Math. Theor. **49**, 30LT01 (2016).

[6] J. Alicea and P. Fendley, Topological phases with parafermions: Theory and blueprints, Annu. Rev. Condens. Matter Phys. **7**, 119 (2016).

[7] J. Kemp, N. Y. Yao, C. R. Laumann, and P. Fendley, Long coherence times for edge spins, J. Stat. Mech.: Theory Exp. (2017) 063105.

[8] D. V. Else, P. Fendley, J. Kemp, and C. Nayak, Prethermal Strong Zero Modes and Topological Qubits, Phys. Rev. X **7**, 041062 (2017).

[9] L. M. Vasiloiu, F. Carollo, and J. P. Garrahan, Enhancing correlation times for edge spins through dissipation, Phys. Rev. B **98**, 094308 (2018).

[10] L. M. Vasiloiu, F. Carollo, M. Marcuzzi, and J. P. Garrahan, Strong zero modes in a class of generalized Ising spin ladders with plaquette interactions, Phys. Rev. B **100**, 024309 (2019).

[11] D. J. Yates, F. H. L. Essler, and A. Mitra, Almost strong $(0, \pi)$ edge modes in clean interacting one-dimensional Floquet systems, Phys. Rev. B **99**, 205419 (2019).

[12] D. J. Yates, A. G. Abanov, and A. Mitra, Lifetime of Almost Strong Edge-Mode Operators in One-Dimensional, Interacting, Symmetry Protected Topological Phases, Phys. Rev. Lett. **124**, 206803 (2020).

[13] J. Kemp, N. Y. Yao, and C. R. Laumann, Symmetry-Enhanced Boundary Qubits at Infinite Temperature, Phys. Rev. Lett. **125**, 200506 (2020).

[14] D. J. Yates, A. G. Abanov, and A. Mitra, Dynamics of almost strong edge modes in spin chains away from integrability, Phys. Rev. B **102**, 195419 (2020).

[15] D. J. Yates and A. Mitra, Strong and almost strong modes of Floquet spin chains in Krylov subspaces, Phys. Rev. B **104**, 195121 (2021).

[16] D. Yates, A. Abanov, and A. Mitra, Long-lived period-doubled edge modes of interacting and disorder-free Floquet spin chains, Commun. Phys. **5**, 43 (2022).

[17] L. M. Vasiloiu, A. Tiwari, and J. H. Bardarson, Dephasing-enhanced Majorana zero modes in two-dimensional and three-dimensional higher-order topological superconductors, Phys. Rev. B **106**, L060307 (2022).

[18] K. Klobas, P. Fendley, and J. P. Garrahan, Stochastic strong zero modes and their dynamical manifestations, Phys. Rev. E **107**, L042104 (2023).

[19] L. Jiang, T. Kitagawa, J. Alicea, A. R. Akhmerov, D. Pekker, G. Refael, J. I. Cirac, E. Demler, M. D. Lukin, and P. Zoller, Majorana Fermions in Equilibrium and in Driven Cold-Atom Quantum Wires, Phys. Rev. Lett. **106**, 220402 (2011).

[20] M. Thakurathi, A. A. Patel, D. Sen, and A. Dutta, Floquet generation of Majorana end modes and topological invariants, Phys. Rev. B **88**, 155133 (2013).

[21] D. V. Else and C. Nayak, Classification of topological phases in periodically driven interacting systems, Phys. Rev. B **93**, 201103(R) (2016).

[22] R. Roy and F. Harper, Abelian Floquet symmetry-protected topological phases in one dimension, Phys. Rev. B **94**, 125105 (2016).

[23] V. Khemani, A. Lazarides, R. Moessner, and S. L. Sondhi, Phase Structure of Driven Quantum Systems, Phys. Rev. Lett. **116**, 250401 (2016).

[24] A. C. Potter, T. Morimoto, and A. Vishwanath, Classification of Interacting Topological Floquet Phases in One Dimension, Phys. Rev. X **6**, 041001 (2016).

[25] H.-C. Yeh, G. Cardoso, L. Korneev, D. Sels, A. G. Abanov, and A. Mitra, Slowly decaying zero mode in a weakly non-integrable boundary impurity model, arXiv:2305.11325.

[26] P. Jung, R. W. Helmes, and A. Rosch, Transport in Almost Integrable Models: Perturbed Heisenberg Chains, Phys. Rev. Lett. **96**, 067202 (2006).

[27] P. Jung and A. Rosch, Spin conductivity in almost integrable spin chains, Phys. Rev. B **76**, 245108 (2007).

[28] P. Jung and A. Rosch, Lower bounds for the conductivities of correlated quantum systems, Phys. Rev. B **75**, 245104 (2007).

[29] D. V. Else, B. Bauer, and C. Nayak, Prethermal Phases of Matter Protected by Time-Translation Symmetry, Phys. Rev. X **7**, 011026 (2017).

[30] D. A. Abanin, W. De Roeck, and F. Huveneers, Exponentially Slow Heating in Periodically Driven Many-Body Systems, Phys. Rev. Lett. **115**, 256803 (2015).

[31] D. Abanin, W. De Roeck, W. W. Ho, and F. Huveneers, A rigorous theory of many-body prethermalization for periodically driven and closed quantum systems, Commun. Math. Phys. **354**, 809 (2017).

[32] X. Mi *et al.*, Noise-resilient edge modes on a chain of superconducting qubits, Science **378**, 785 (2022).

[33] A. Matthies, J. Park, E. Berg, and A. Rosch, Stability of Floquet Majorana Box Qubits, Phys. Rev. Lett. **128**, 127702 (2022).

[34] D. D. Vu, R.-X. Zhang, Z.-C. Yang, and S. Das Sarma, Superconductors with anomalous Floquet higher-order topology, Phys. Rev. B **104**, L140502 (2021).

[35] A. K. Ghosh, T. Nag, and A. Saha, Floquet generation of a second-order topological superconductor, Phys. Rev. B **103**, 045424 (2021).

[36] A. Mitra, H.-C. Yeh, F. Yan, and A. Rosch, Nonintegrable Floquet Ising model with duality twisted boundary conditions, Phys. Rev. B **107**, 245416 (2023).